Particle Accelerators, 1992, Vol. 40, pp.17–41
Reprints available directly from the publisher
Photocopying permitted by license only

DESIGN CHALLENGES FOR HIGH CURRENT STORAGE RINGS*

H. PADAMSEE, P. BARNES, C. CHEN, W. HARTUNG, J. KIRCHGESSNER, D. MOFFAT, R. RINGROSE, D. RUBIN, Y. SAMED, D. SARANITI, J. SEARS, Q.S. SHU and M. TIGNER

Laboratory of Nuclear Studies, Cornell University

High luminosity e^+e^- and pp colliders stand to gain from the use of superconducting RF systems (SRF). To achieve luminosities $> 3 \times 10^{33}$ in a B-factory, 1 - 2 amps of current must be stored in several 100 bunches, spaced a few meters apart. Similarly the LHC p-p ring aims to store $\sim$ 1 amp in nearly 5000 bunches, spaced 5 meters apart. Such high currents make it imperative to lower the impedance of the rings, of which RF cavities are a major source. The tight bunch spacing makes control of multibunch instabilities one of the most important issues. The advantage of using SRF cavities for high luminosity machines is that they can economically provide higher gradients than copper cavities. Hence, by minimizing the structure length, they can sizably reduce the machine impedance. In superconducting cavities, the need to use small beam holes and re-entrant iris shapes to maximize the shunt impedance of the accelerating mode is eliminated by virtue of the high Q. SRF cavity shapes can be chosen to tolerate reduced impedance in the accelerating mode, while substantially cutting the impedance of all the higher order modes. As an added bonus, capital and operating cost savings can be realized from the reduced RF installation which no longer needs to provide for RF power dissipation in the cavity walls. To operate in future high current machines, SRF cavities developed for the present generatioan of e^+e^- storage rings need to be advanced in several respects, in particular their input and output power handling capabilities, and the damping of higher order modes. Progress in meeting these challenges in the context of specific application of SRF to the Cornell B-factory, CESR-B is discussed.

1 INTRODUCTION

The luminosity and energy frontiers for e^+e^- colliders are shown in Fig. 1.[1] Application of SRF at the energy frontier is discussed in other papers at Hamburg SRF/TESLA workshop. On the luminosity frontier, the Phi factory at Frascatti is approved and the Tau-Charm Factory is under consideration for Spain. Several proposals for B-factories are now under consideration for Cornell, SLAC, KEK, Novosibirsk, CERN and DESY.

All schemes are based on storing beam currents of 1 – 2 amps, compared to the maximum of 150 mA ever stored in an e^+e^- ring.[2] An advanced SRF cavity suitable for a B-factory would also be attractive for the Tau-Charm factory[1] and for high luminosity, high current proton-proton colliders such as the LHC, and possibly even for the SSC. For the SSC it has been estimated[3] that the use of PEP type NC cavities would result in a multibunch instability rise time of 1 sec, which is very fast compared to the radiation

* Supported by the National Science Foundation with Supplementary Support from the US-Japan Collaboration

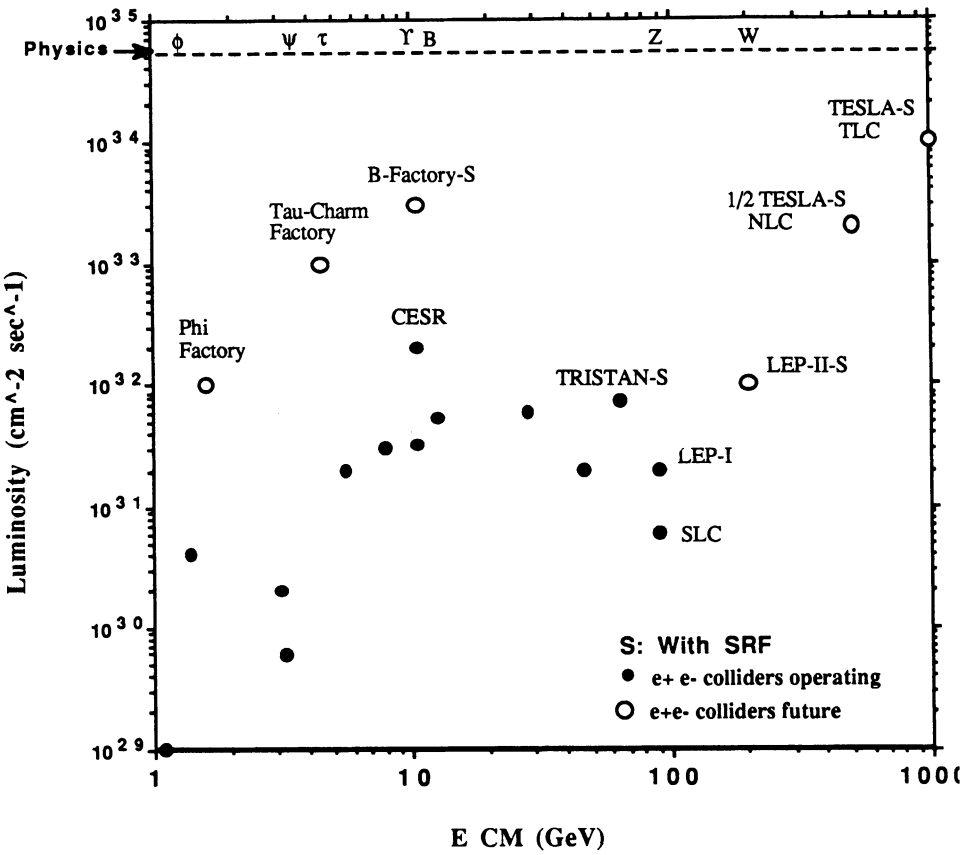

FIGURE 1: The luminosity and energy frontiers for e^+e^- colliders.

damping time of 13 hours. One worry is that the customary approach of feedback control of this instability could lead to emittance blow up as observed at Fermilab. Table 1 compares the relevant parameters for high luminosity machines which stand to benefit from SRF.

2 THE CASE FOR SUPERCONDUCTING RF CAVITIES

To avoid single- and multi-bunch instabilities with such high currents, it is essential to lower the impedance of the rings. RF cavities are a chief source of impedance. The advantage of using SRF is that higher gradients (5 – 10 MV/m) are possible than with room temperature RF (1 – 2 MV/m), allowing a substantial reduction in the number of cells and their corresponding impedance. SRF cavity shapes can be optimized for low impedance in the higher order modes (HOM) by choosing a large beam pipe and a smooth iris geometry. Unlike normal conducting cavities, the resulting loss in shunt impedance of the accelerating mode can be tolerated because the Q is 10^5 times higher.

TABLE 1: Selected parameters for high luminosity machines which stand to benefit from SRF

	CESR-B B-Factory	Tau-Charm Factory	LHC	SSC
Beam Current (A)	1–2	0.5	0.85	0.072
Voltage (MV)	47	64	16	40
No. of Bunches	230	21	4725	17,000
Bunch Sep (m)	3.3	16	4.5	5

TABLE 2: Comparison between a possible normal conducting and the envisioned superconducting RF system for the CESR-B factory

	LER	HER
Voltage (MV)	12	35
Beam Power (MW)	1.5	4.5
Normal Conducting		
Gradient (MV/m)	1	1
No. of cells	40	117
Cavity dissipation (MW)	3.4	9.8
Superconducting		
No. of cells	4	12
Gradient (MV/m)	10	10
Cavity dissipation (watts) ($Q = 1 \times 10^9$)	408	1224

Furthermore, because of superconductivity, there is a substantial savings in capital cost from the smaller RF installation which needs to only provide the beam power, the cavity dissipation being negligible. Corresponding savings in operating cost are realized. These advantages are accentuated by the need for short bunches, which demand higher voltages. A quantitative comparison between a possible normal conducting RF system for a machine such as CESR- B[4] and the SRF system envisioned is presented in Table 2. A parameter list for CESR-B is listed in Appendix A.

3 CELL SHAPE

All storage ring applications of SRF to date are based on multicell cavities. An attractive approach to meet the power requirements accompanying ampere size currents is to reduce the input and output coupler loads by distributing the power to be handled over many single-cell cavities. This approach also lends itself to maximal higher mode damping.

After extensive URMEL[9] studies of cell shapes with varying iris radii, cell length and beam pipe radii, a new cell shape has been chosen to reduce the impedances of higher order modes and to facilitate power extraction and strong damping. Fig. 2 shows the

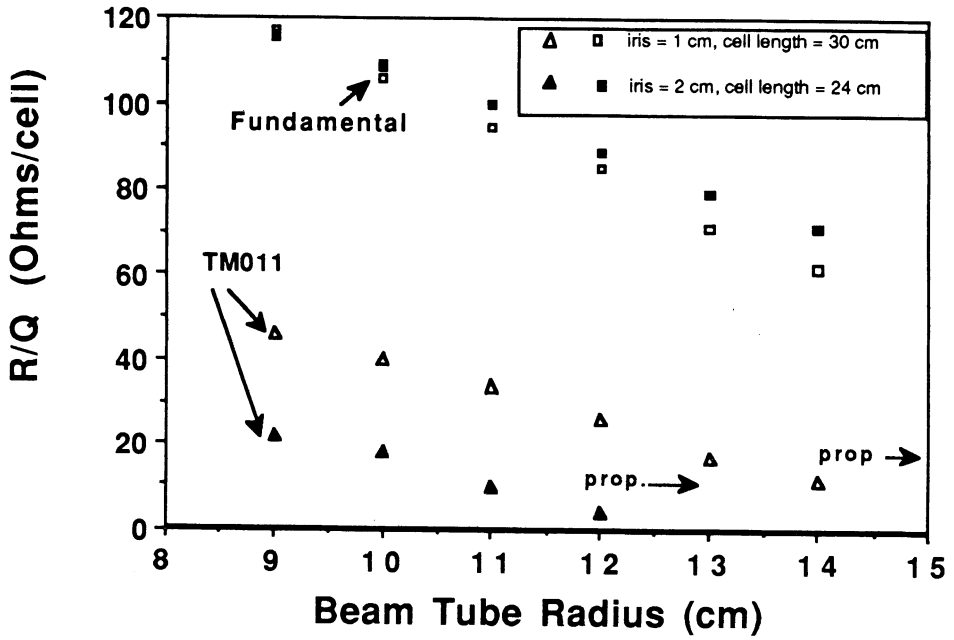

FIGURE 2: Reduction of impedance of the most dangerous HOM by varying cell shape.

drop in the R/Q vs. beam pipe radius of the worst longitudinal HOM (TM011) along with the R/Q of the fundamental. Two illustrative choices of iris radius and cell length are presented. Note that the loss in accelerator mode R/Q is not severe over the range studied. Above 12 cm beam pipe radius, the better choice (2 cm iris radius, cell length of 24 cm) showed that the TM011 mode starts to propagate freely down the beam pipe.

Fig. 3 compares the new cell shape with a typical normal conducting cell shape (eg. presently used in CESR) and with the superconducting cavity shape that is planned for LEP-II. The overall parasitic mode loss factor as determined by TBCI[10] has been reduced by a factor of 3 over the NC shape and a factor of 2 over LEP-II.[11]

A major advance provided by the new shape is that the impedance of the most dangerous HOMs have been reduced by large factors as compared to the typical shape of a NC cavity. Fig. 4 compares the R/Qs of a NC cell shape with the proposed CESR-B SC cell shape. For longitudinal HOMs, the upper graph shows that the highest impedance has been reduced by more than a factor of 10. The comparison for dipole HOMs is shown in the lower graph. Here again there is a major reduction in impedance for all but the first two transverse modes.

Another major advance provided by the new shape is that all longitudinal HOMs propagate out of the cavity via a round beam pipe. This was confirmed by examining the field profile in the beam pipe as computed by URMEL for all TM0,m,n modes up to 5 GHz. This feature allows all HOM coupling devices to be placed outside the liquid helium cryostat, greatly simplifying high power extraction and damping.

Similarly it was determined that all deflecting modes (TM1,m,n and TE1,m,n modes

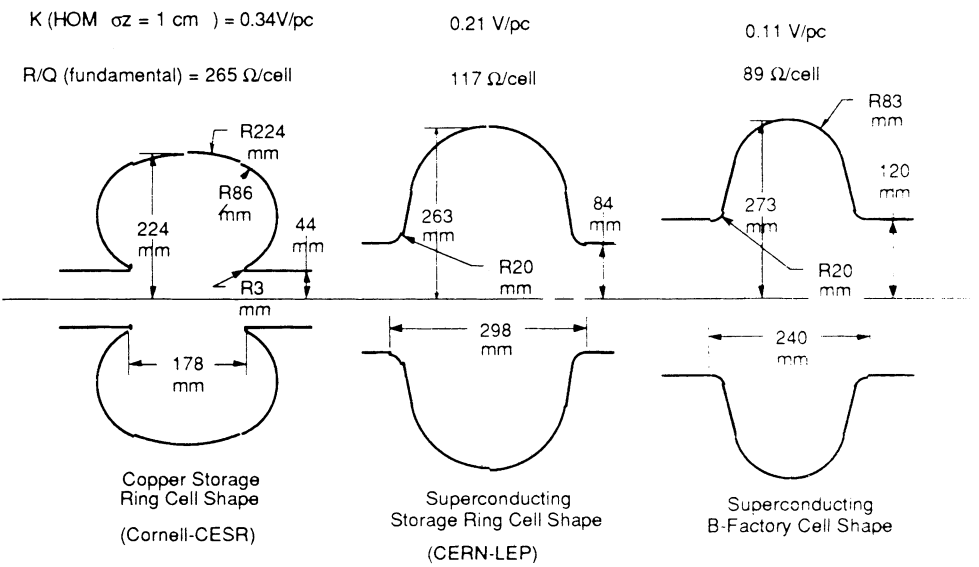

FIGURE 3: A comparison of NC and SC cell shapes used for storage ring cavities.

TABLE 3: Properties of Non-propagating deflecting modes. R'/Q is defined as $(R/Q)/(kr0)^2$ where $k = \omega/c$ and R/Q is the longitudinal shunt impedance at a distance $r0$ off axis.

Mode	Frequency MHz	R'/Q Ohms/cell
TE111	644	2.8
TM110	680	25

up to 4 × fundamental frequency) also propagate out the beam pipe, except for the two lowest frequency transverse HOMs. These are the TE111 and the TM110 modes. Their properties are listed in Table 3.

To extract these "trapped" modes, we consider the use of a fluted beam pipe of cross-section similar to that shown in Fig. 5, following an idea of Kageyama.[12]

Using URMEL in the waveguide calculation mode, we calculated the TE11 cut-off frequency of a fluted beam pipe of various cross sections as defined by a width (w) and height (h). (Fig. 6)

Because of the beam hole, the TM110 cavity mode is partially TE111-like. Thus both trapped modes (TM110 and TE111) couple to the fluted beam pipe via the TE11 waveguide mode, and it is only necessary to lower the propagation frequency of the TE11 mode to below that of the two trapped cavity modes. It is desirable to keep the height of the flutes reasonable compared to the diameter of the cell, and the width of the flute small enough to avoid an intolerable increase in the loss factor. A suitable flute geometry is finally chosen based on the feasibility of fabrication.

MAFIA[13] calculations show that the rectangular waveguides formed by the flutes

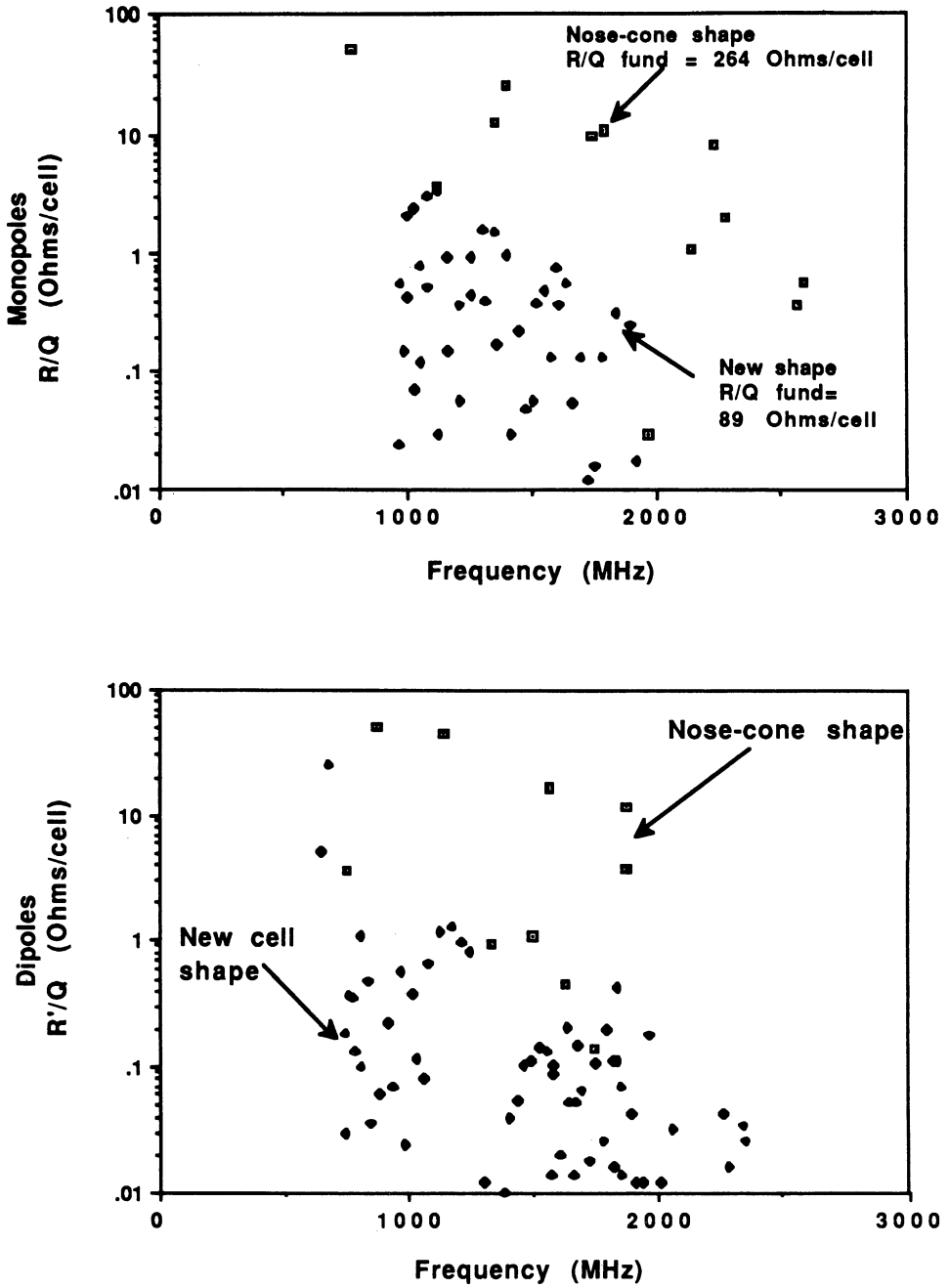

FIGURE 4: A comparison of impedances of the CESR-B cell shape with impedances of a NC cavity cell shape. Note that while the B shape has the fundamental R/Q lower by a factor of 3, the R/Q for the higher modes are lower by much larger factors

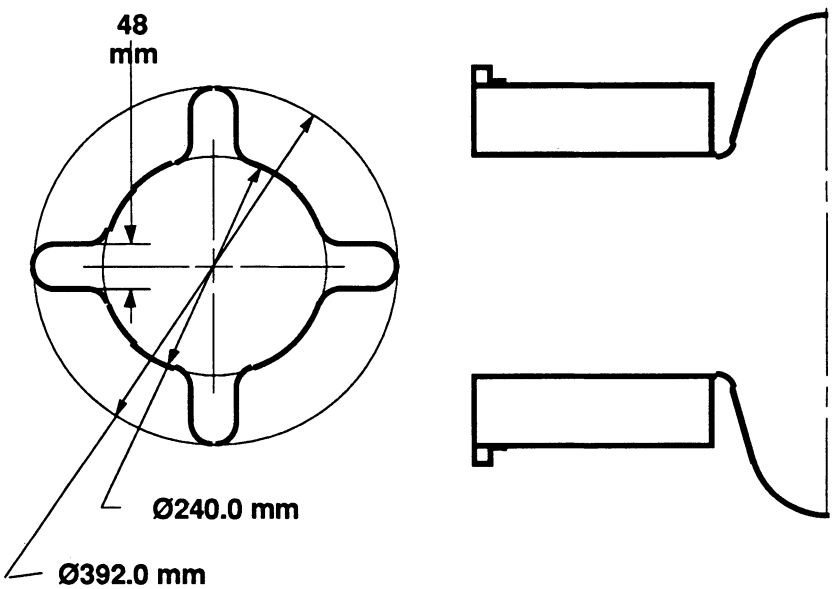

FIGURE 5: Geometry of fluted beam pipe

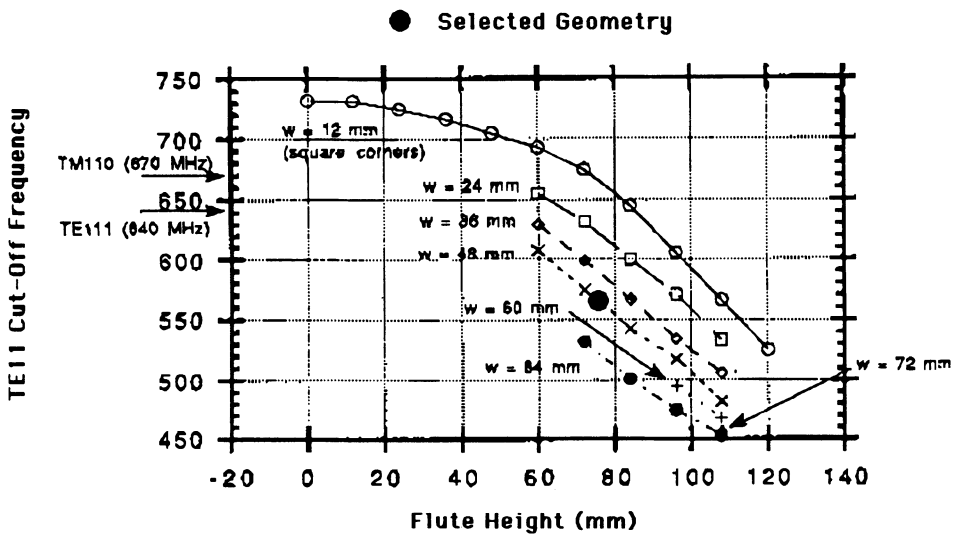

FIGURE 6: Cut-off frequency of the TE11 mode in fluted beam pipes of various geometries.

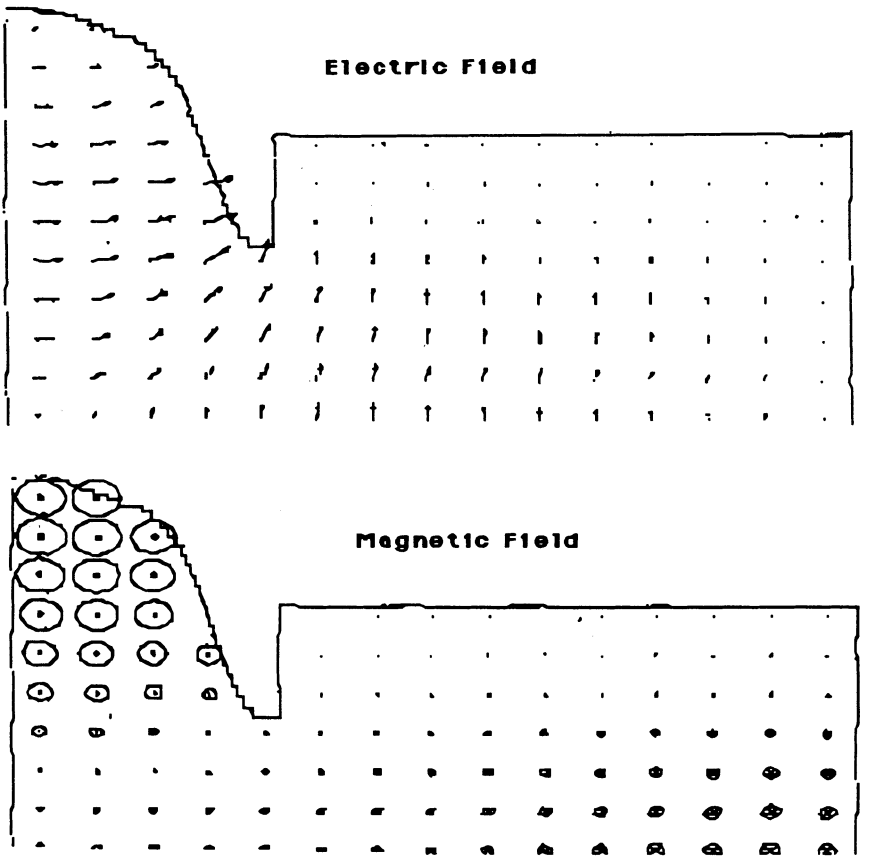

FIGURE 7: Electric and magnetic fields calculated by MAFIA for the CESR-B cell with a fluted waveguide.

serve to guide out the troublesome transverse modes. The electric and magnetic field configurations calculated by MAFIA for the TM110 mode is shown in Fig. 7. Note the excellent propagation out the fluted beam pipe.

For an ideal cell shape, we do not expect the fundamental mode to propagate out the fluted beam pipe. However, slight misalignments may introduce TE11 like components in the TM010 mode. For the flute geometry chosen, the TE11 cut-off frequency is $\sim$ 570 MHz, so that the fundamental mode will still be cut off. For a 3 GHz copper model, the power attenuation of the fundamental mode in the fluted as well as the round beam pipe measured 9 db/cm as compared with URMEL prediction for a round beam pipe of 10 db/cm. Another concern is that the presence of the flutes will increase the loss factor, as the flutes chosen occupy 1/4 of the beam pipe circumference. MAFIA calculation of the loss factor for the chosen flute geometries (without cavity) showed only a 10% increase in total cavity loss factor at 1 cm bunch length.

4 HIGHER MODE COUPLERS

Because of good HOM propagation via the large diameter fluted beam pipe, the beam pipes are considered as the best HOM conduits. This approach addresses the need to increase the power handling capability of the HOM couplers. We consider placement of the HOM couplers outside the cryostat, and on the beam pipe.

A conceptually simple scheme to achieve strong damping is to replace a small section of the beam pipe outside the cryostat with a strong absorber material. Interaction with the beam is likely to be minimal in view of the large diameter (24 cm) of the pipe. As a computational exercise, we considered a 15 cm long absorptive band with RF surface resistance 10^4 times copper. Using URMEL (variable mesh, 150,000 mesh points) to compute the fields in the region of the absorber, calculated Qext values are shown in Fig. 8 for monopole and dipole modes up to $\sim$ 2.5 GHz. The cell geometry used for these calculations is shown in Fig. 9. The low Qs shows that all the modes propagate well. Qext values obtained for a real absorber will be measured on a full scale model.

A promising absorbing material, called Ferrite-50, has been found to have the desired loss properites. A complete discussion of its properties is presented in Section 8.

There is now a computer program based on SUPERFISH[14] called SEAFISH,[15] which allows input of material parameters in segments, such as complex ε and μ. With these parameters, SEAFISH can calculate the resonant frequencies, field patterns and Qext of monopole modes for cavities with absorbing materials. Using the preliminary properties of Ferrite-50 discussed in Section 5, we calculated with SEAFISH the frequencies and Qext of several monopole modes. Fig. 9 shows a typical field plot from SEAFISH with and without ferrite. These calculations confirmed that the ferrite material will provide the necessary damping. (These calculations will be redone after refined measurements on ferrite properties are obtained.)

For damping measurements, a 1/6 scale copper cavity model (3 GHz fundamental frequency) with round (non-fluted) beam pipes was equipped with 2.5 cm long Ferrite-50 beam tube sections. These sections were located 7.6 cm away from the cells, which is equivalent to being outside the cryostat. Strong damping ($Q \sim 100$) was observed for all discernable modes (longitudinal and transverse) in the beam pipe region outside the cell. Fig. 10 shows typical results between 5 – 6 Ghz and 18 – 20 Ghz, representing the low and high frequency ends of the spectrum. In each frequency range, results with and without the ferrite tube are presented. These results show the effectiveness of the ferrite as a strong absorber.

To experimentally check the propagation of the trapped transverse modes via a fluted beam pipe, and the effectiveness of ferrite damping for these modes, another 1/6 scale model was built but equipped with a fluted pipe on one side. The other side was kept non-fluted to avoid mechanical entanglement with the input coupler (see Section 7).
Mode spectra between 3.5 and 4.2 GHz (580 – 700 MHz equivalent) are shown in Fig. 11 (a) without the fluted tube, 11 (b) with a fluted beam tube followed by a short at the end, and finally in 11 (c) with the short replaced by a ferrite load. Based on these studies, Q values around 200 are anticipated for the most dangerous deflecting modes. It is planned to repeat these measurements on a full scale copper model, presently under construction.

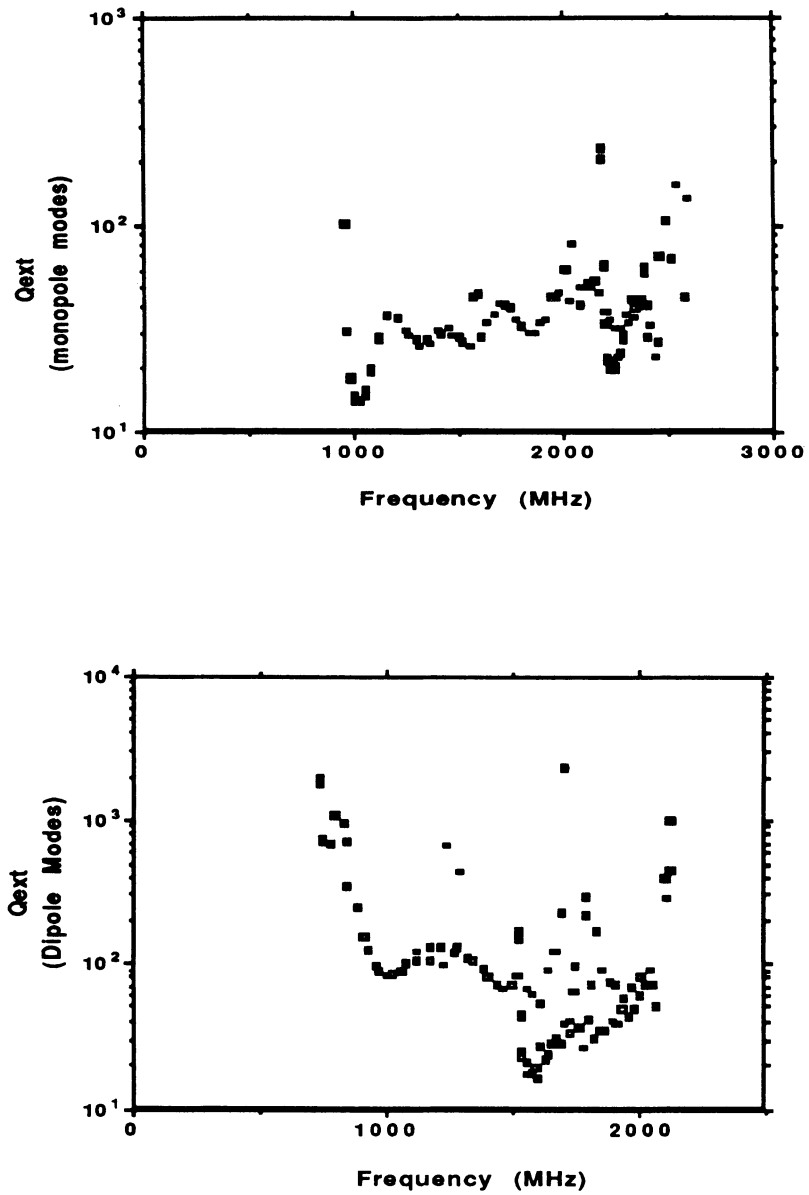

FIGURE 8: Calculated Qext for HOMs based on placing a strong absorber on the beam pipe.

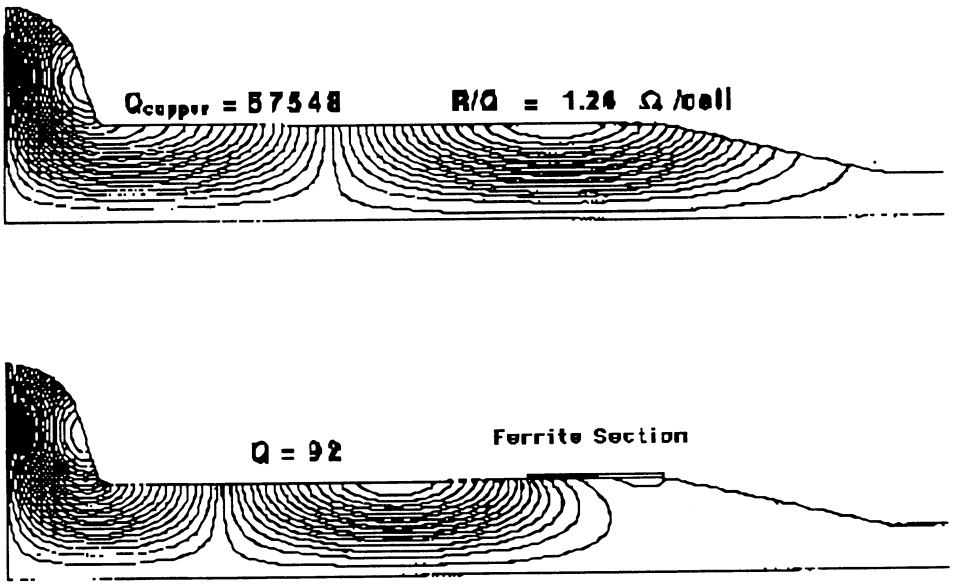

FIGURE 9: Field profiles, and Qext calculated by SEAFISH for a ferrite HOM absorber.

Risetimes of multibunch instabilities were calculated with the program ZAP[16] using 6 monopole higher modes with the highest R/Q values (between 2 – 4 Ohms/cell), each with $Q = 70$. Results showed that there will be no multi-bunch beam instabilities in a machine such as CESR-B, eliminating the need for a longitudinal bunch to bunch feedback system, considered a significant challenge. (For eg the SLAC approach[17] calls for a 240 MHz bandwidth system with a total aimplifier power of 8 kwatts for the HER. Damping of HOMs to Qs of 70 is assumed.) These calculations proved the effectiveness of the alternate strategy of reducing the number of cells, their impedances and Qext values.

ZAP calculations were also carried out for the two highest impedance transverse modes (see Table 3) assuming Qext = 200. Results show that the high energy ring is safe from cavity engendered, transverse multibunch instabilities. However in the low energy, high current ring the instability rise time is shorter (3 msec) than the radiation damping time (27 msec). Hence some transverse feedback will be necessary. For a horizontal feedback system with a bandwidth of 50 MHz sufficient for bunch to bunch feedback, a 100 watt driver amplifier for the LER and a 500 watt driver amplifier for the HER will be adequate to damp 4mm perturbation in 1 msec. For the vertical feedback system, a 2 watt amplifier for the LER and a 20 watt amplifier for the HER will provide damping of a 2mm perturbation in 1 msec. These drive amplitudes are not formidable and consistent with the present CESR feedback system.[4]

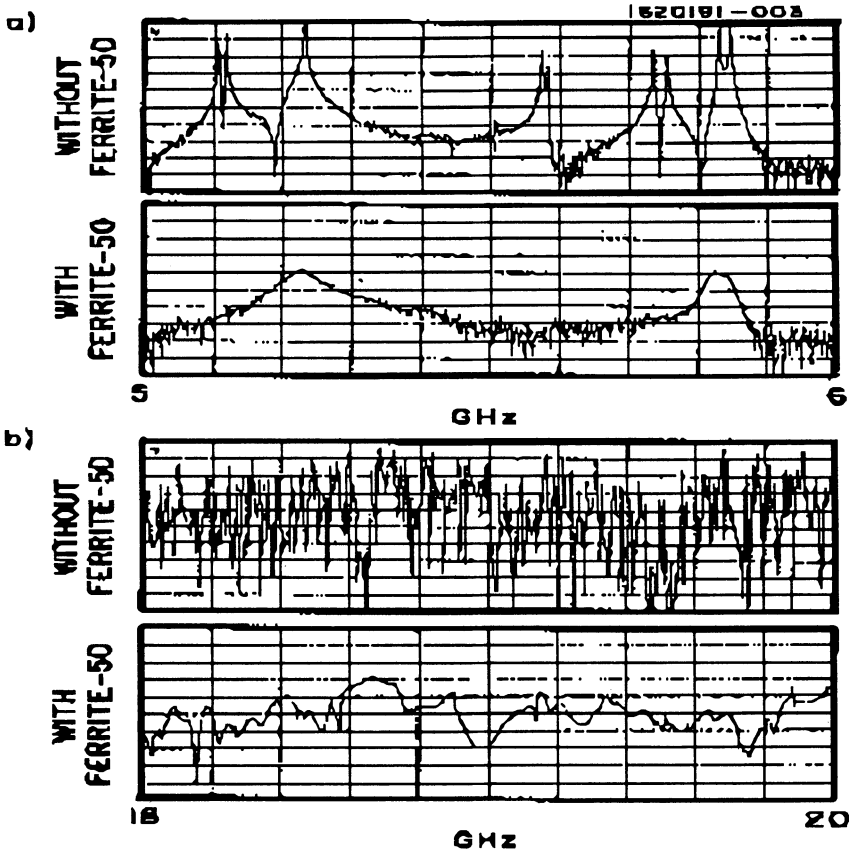

FIGURE 10: Transmitted power vs. frequency over two representative ranges:(a) 5–6 GHz and (b) 18 – 20 GHz. Input and pick-up loops oriented to intercept $H\phi$ were placed on the beam pipe outside the cell. For each frequency range, two curves are presented. The upper is for metallic plates (shorts) placed at the ends of the cryostat. The lower is for ferrite beam tube loads replacing the shorts.

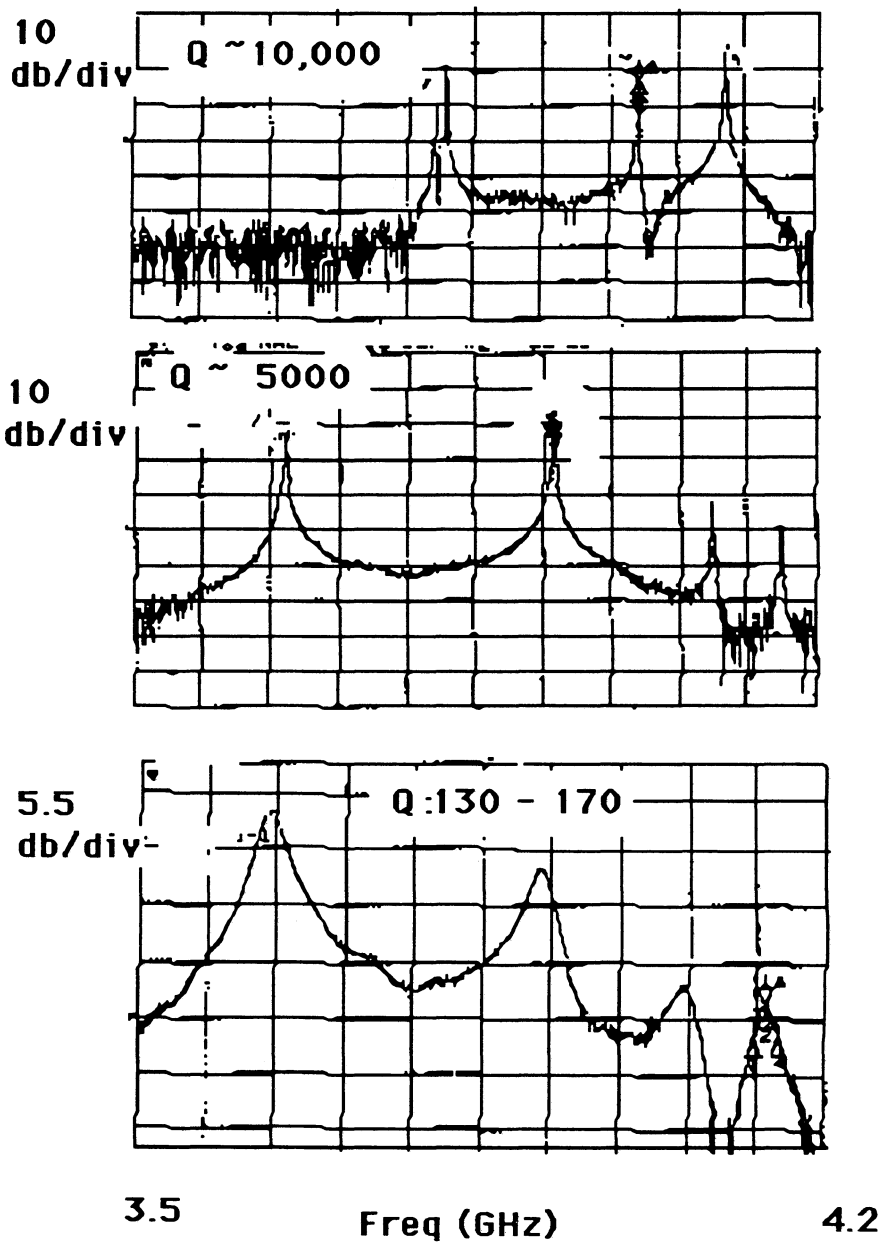

FIGURE 11: Damping of the TM110 and TE111 modes by ferrite. The upper graph shows the frequency and Q s of the undamped modes in a cell with round beam pipes. Q s are highest because the modes are trapped in the cell. The middle graph shows the same modes for a cell with fluted beam pipes terminated by a short. Q s are somewhat lower because of contact losses at the shorting plate. The bottom graph shows the same modes now damped with a ferrite beam tube at the end of the fluted beam pipe.

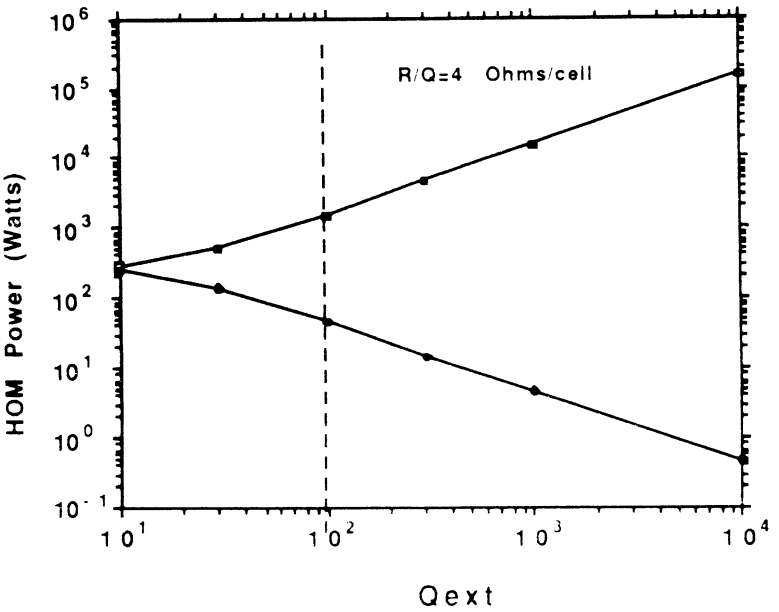

FIGURE 12: Resonant and antiresonant excitation of a higher order mode with $R/Q = 4$ Ohms/cell.

5 HIGHER MODE POWER

If the Q of the higher order modes is $<< \omega Tb/2$, where ω is the HOM angular frequency and Tb the bunch spacing, then the power deposited by the beam in a cell is given by:[18]

$$P\text{HOM} = k(Ne)^2\, nb\ \text{frev}$$

where k is the loss factor of the cell, N is the number of particles per bunch, nb the number of bunches = 230 and frev the revolution frequency = 3.9×10^5 Hz. At 1 cm bunch length, with HOM loss factor of 0.1 V/pC, the power loss will be 0.8 Kwatts/cell and 4.3 kWatts/cell for the high and low energy rings. Since the bunch spacing for the various rings is $\sim$ 10 nsec, the condition on the Q to obtain the limiting power is extreme, ie $Q << 20$. Therefore even for $Q \sim 100$, we expect some of the HOMs to be excited resonantly and some anti-resonantly. In the worst case, if one of the lines of the beam current spectrum falls exactly on a "weakly" damped cavity resonance, then there will be maximum resonant excitation of as much as 1.5 kwatts in this higher order mode as shown in Fig. 12.

Using the impedances shown in Fig. 4 and the frequencies calculated by URMEL, the statistical distribution of power deposited in the various modes for one set of frequencies was calculated[18] and is shown in Fig. 13. The total power for the LER is 4 kwatts. Some safety margin is necessary to allow for deviations.

The image current wall losses which are estimated to be < 1 kwatt per section, from the resistivity of the ferrite. The total power for each ferrite section is then expected to be well below 10 kwatts, corresponding to a power density of 10 watts/cm^2.

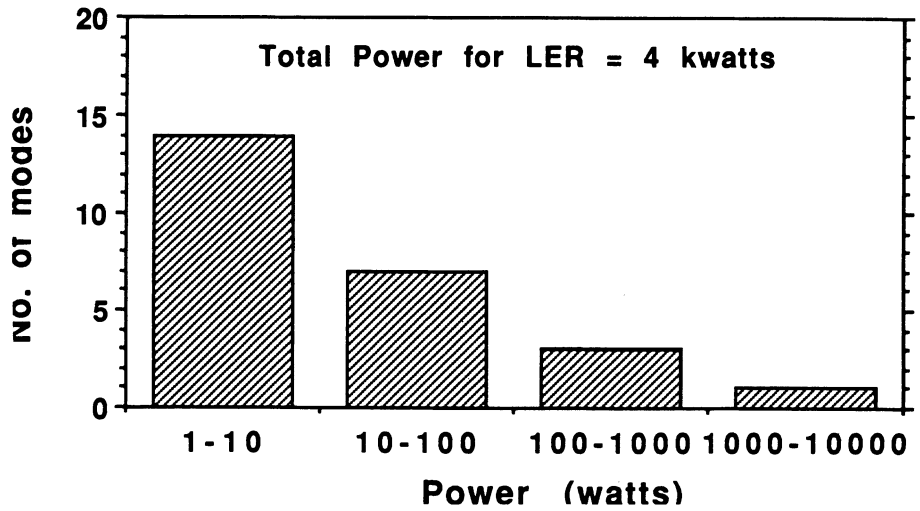

FIGURE 13: Distribution of beam power deposited in higher modes for one particular set of frequencies, as calculated by URMEL.

6 FERRITE PROPERTIES

The HOM load design places the following demands on the material to be used:

- RF resistivity $\approx 10^4\times$ copper
- use in a vacuum $\leq 10^{-9}$ torr
- electrically and thermally conducting
- broad-banded load able to handle the dissipation of ~ 10 W/cm^2

We have identified Ferrite-50 (Transtech, Inc. Adamstown, MD) as a candidate material for this use. This ferrite has a μ at 1 kHz > 150 and a nominal DC resistivity of ~ 25 Ω-cm. An alternate ferrite made by the same company is TT2211/R. In order to evaluate the suitability of either ferrite for our purposes we determined the following properties:

- complex ε_r and μ_r as a function of frequency
- bondability
- vacuum compatibility
- power handling capability

The most common definitions of complex ε and μ are:

$$\varepsilon = \varepsilon_O \varepsilon_r = \varepsilon_O(\varepsilon' - j\varepsilon'')\mu = \mu_O \mu_r = \mu_O(\mu' - j\mu'')$$

We used a coaxial test line connected to an HP 8720A network analyzer to measure the real and imaginary parts of ε_r and μ_r from 0.2 to 20 GHz. The procedures and equations

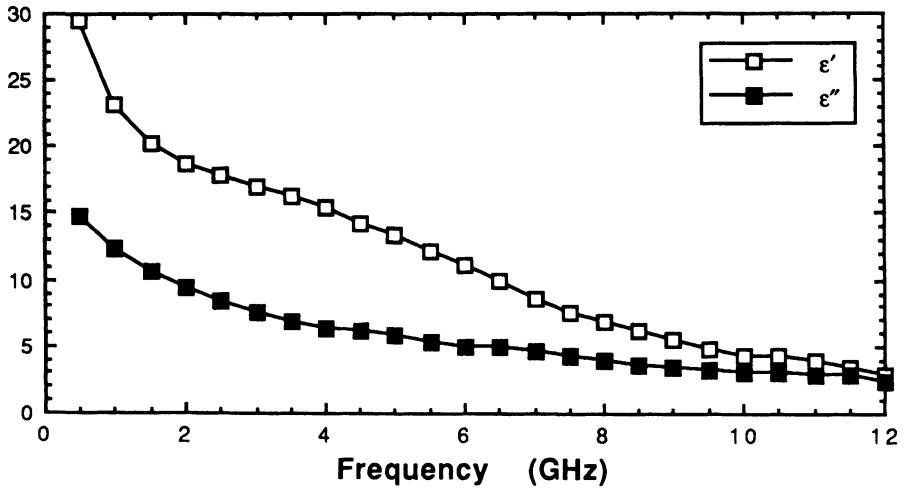

FIGURE 14: Measured values of ε_r for Ferrite-50.

necessary to determine ε_r and μ_r from the S-parameters are given in Ref. 19. To verify that our apparatus was yielding accurate results, a 6.5 mm piece of teflon was measured. The measured values of $\varepsilon' \sim 2.0$ and $\mu' \sim 1$ were quite close to the accepted values over the frequency range 0.5 – 10 GHz. The measurements of ε'' and μ'' deviated from their expected values for teflon. This resulted, in part, because the technique does not measure low-loss materials accurately. Our apparatus is also in need of an improved calibration set, which is being procured. While awaiting refinements, we measured a 3.6 mm piece of Ferrite-50. Our preliminary results are shown in Figs. 14 and 15.

Knowledge of ε_r and μ_r as a function of frequency allows one to calculate parameters such as skin depth, loss tangent, impedance, etc. Figure 16 shows the frequency dependence of the skin depth and Fig. 17 shows the real part of the impedance of Ferrite-50 calculated using our measured values of ε and μ.

A bead of Ferrite-50, when placed on the axis of a copper cavity lowered the Q from 40,000 to 1400. SEAFISH calculations using ε and μ predicted that a bead of the same size would lower the Q to 2345, in fair agreement with measured values.

ε and μ values of the alternate TT2211/R ferrite are reported in the literature.[20] Magnetic loss properties are comparable to Ferrite-50. However this ferrite has a lower dielectric loss factor. When a bead was placed on the axis of a copper accelerating cell it hardly lowered the Q of a copper cavity from 40,000, but substantially dropped the Q when placed near the equator. SEAFISH calculations for damping of two HOMs with TT2211/R gave Qext near 100, comparable to results with Ferrite-50. Further measurements are necessary over a broad spectrum of HOMs to determine if the mode damping properties of this ferrite are acceptable. A possible disadvantage is that the DC resistivity is 10^4 Ohms-cm. On the other hand, TT2211/R has superior mechanical properties and allowed excellent vacuum when used in the ACOL ring at CERN.

The present concept is to bond ferrite tiles to a metallic shell which is water cooled. The shell must be made of a material with thermal expansion coefficient close to that of

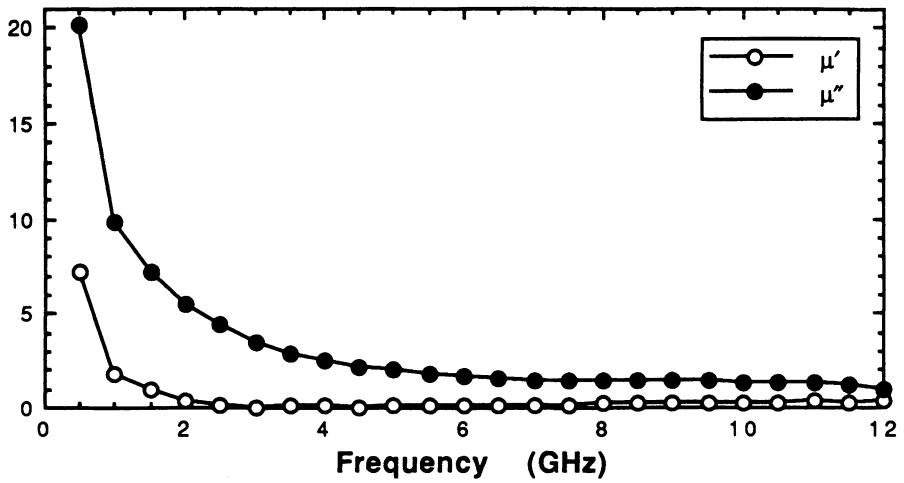

FIGURE 15: Measured values of μ_r for Ferrite-50.

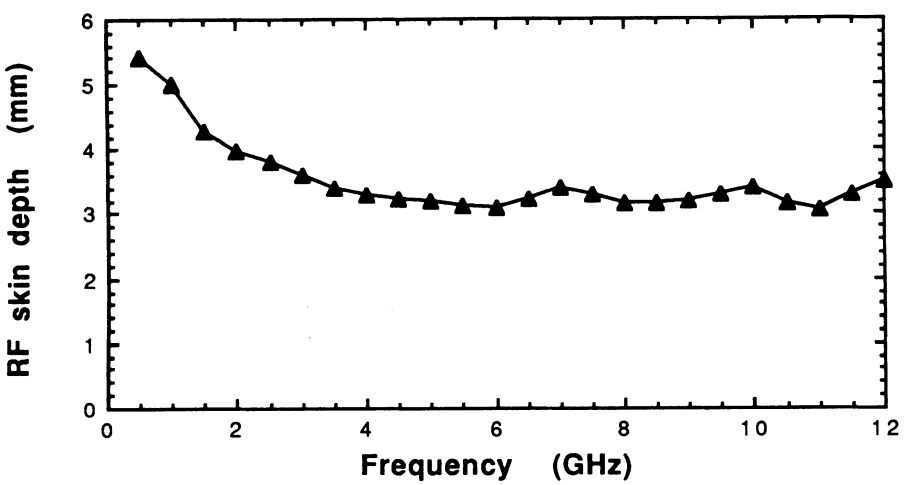

FIGURE 16: Skin depth from measured e and μ.

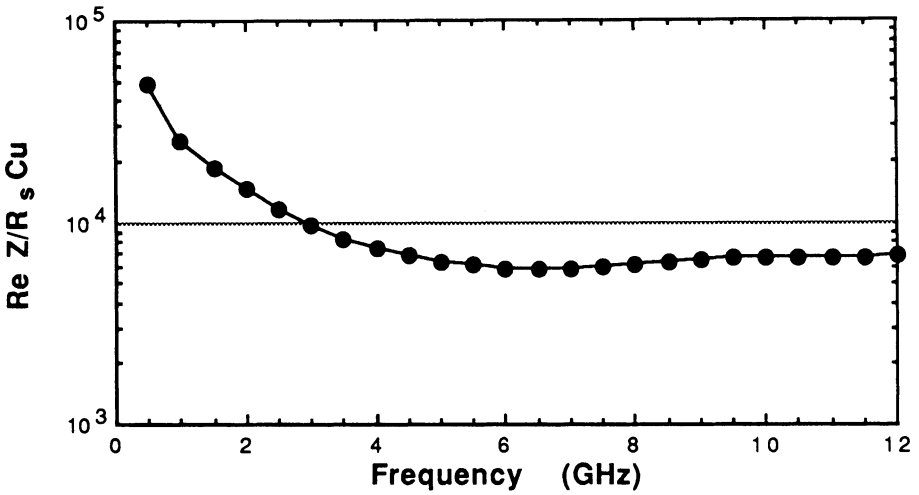

FIGURE 17: Frequency dependence of the real part of the impedance of Ferrite-50 divided by the surface resistivity of copper.

ferrite, such as titanium, or a 400-series stainless steel. After some trial and error, we discovered a bonding agent that worked well for Ferrite-50, PYRO-DUCT 597. (Aremco, Inc., Ossining, NY) It consists of an aquaeous-based inorganic binder which is loaded with silver flakes. When cured, i.e. when the water is driven off, the result is a conducting ceramic which can be used at temperatures as high as $\sim$ 900°C. Both the metal substrate and ferrite pieces are sand-blasted to permit a good bond. Both types of ferrite retain their loss properties after 800 C bake, as demonstrated by cavity Q measurements.

A sample piece of Ferrite-50 bonded to 410 stainless steel was tested for vacuum compatibility. The sample and system were baked at 325°C for several hours. The vacuum of the system after this was limited by the pump to $\sim 3 \times 10^{-9}$ torr. An outgassing rate of $\sim 2 \times 10^{-10}$ torr-l/sec was determined by turning off the pump for 2.5 hours and measuring the increase in pressure.

For high power tolerance of the ferrite, we placed a Ferrite-50 tube at a magnetic field maximum in a resonant TEM cavity made from $1^5/_8$ inch coax. The dimensions of the load were 45 mm ID $\times$ 52 mm OD $\times$ 30 mm. The resonant frequency of the cavity is 2450 MHz. The power source for the apparatus was a magnetron from a kitchen microwave oven. At a power density of 10.7 W/cm^2 the ferrite tube began to show cracking. These tests show that a 15 cm long ferrite load will handle 10 kwatts of power.

7 FUNDAMENTAL MODE

Table 5 lists the properties of the fundamental mode as computed by SUPERFISH.

We strive to place the couplers on the beam pipe, outside the cell, so as not to perturb the ideal fields within the cells, which have special anti-multipacting shapes, evolved over

TABLE 4: Properties of the fundamental mode

Frequency	500	Mhz
R/Q	89	Ohms/cell
k(fund.)	0.07	V/pC
Emax/Eacc	2.5	
Hmax/Eacc	51.6	Oe/MV/m
Dissipation	102	Watts/cell
($Q = 1 \times 10^9$, Eacc = 3 MV/cell)		

years of development. This choice also avoids the surface magnetic field enhancement from holes that could lead to premature thermal breakdown. Because of the high powers involved, we are considering a waveguide coupler. In comparison to a coaxial coupler, a waveguide has low power densities and needs only outer wall cooling, which can be accomplished by cold gas heat exchangers similar to those planned for the beam tubes. The overall size and static heat load is reduced somewhat by using a half-height guide.

A design of the coupling iris between the cavity and the waveguide has been developed (see Fig. 18).

Bench tests on a 3000 MHz copper model show QL as low as 5×10^4 can be achieved with this type of slot. Coupling can be reduced by opening the slot gap. Computations with MAFIA show that the increase in loss factor from the coupling slot to be only a few %, which is very encouraging, considering the strong coupling provided. The peak electric and magnetic fields at the coupling slot are $E = 6$ MV/m and $H = 110$ Oe as determined by MAFIA, using a 1/4 wavelength long short to terminate the waveguide. These significant fields are much smaller than the maximum fields in the cell.

The ridged slot coupler used here is a variant of the Scezi coupler.[21] Scezi type couplers have been tested successfully by Karlsruhe in a 1-cell 500 MHz superconducting cavity used for tests in PETRA in the early 1980's.[22] Although these results are encouraging, the detail geometry of our coupler is different. It is important to test the coupler in a full scale cavity. A 500 MHz prototype Nb cavity/coupler has been ordered from industry.

8 HIGH POWER WINDOW

The power handling ability of cavity windows used in NC storage cavities range from 120 to 350 Kwatts.[5] Several coaxial windows are in use on superconducting cavities at 500 MHz up to power levels of 200 Kwatts.

The power level for a cavity window for CESR-B is rather high by these standards. Klystrons have achieved a 1 Mwatt level using coaxial RF vacuum windows. These windows, in spite of their reliability in Klystrons, have not been shown to be easily adapted to application for accelerating cavities. Possible reasons are:

1. The vacuum in Klystrons is usually better than in accelerating cavities.
2. Extreme care is taken with Klystrons to assure that there is very low reflected power back to the Klystron and therefore no standing waves at the window

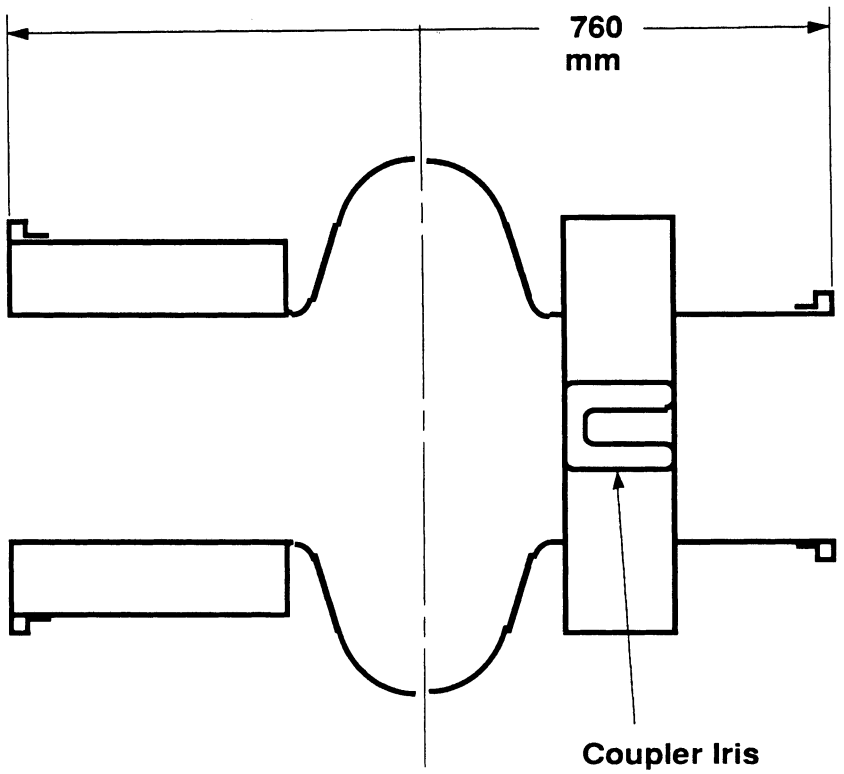

FIGURE 18: Geometry of the coupling iris for the input coupler.

3. In a cavity there may be present HOM power that alters the magnetic and electric fields present at the window, possibly exciting some high frequency resonances associated with the window structure.

In a superconducting accelerating cavity, with heavy beam loading, the input coupling is usually adjusted to be critical ($\beta = 1$), that is, with no reflected power at full beam conditions. In the situation of zero beam current the input is overcoupled and therefore, in the case of superconducting structures, essentially all of the input power is reflected. This assumes that the coupling cannot be dynamically adjusted. This condition of high reflected power cannot be avoided because it exists the time before the beam is injected as well as for a short time after the beam has been lost. The expected P_r (power reflected) versus P_i (incident power) is shown in Fig. 19.

In this curve, any input power level above 125 Kwatts would maintain the cavity voltage and would be capable of maintaining increasing amounts of beam currents. The curve assumes that the coupling has been set to $\beta = 1$ corresponding to input power of 500 Kwatts.

The other requirement is that the VSWR of the window be low in order to avoid loss of incident power as well as to prevent window damage due to heating or arcing.

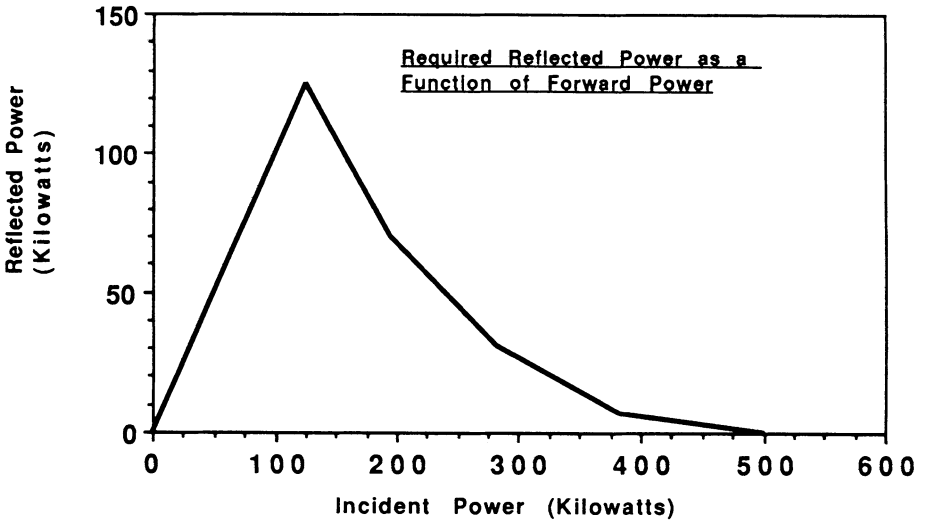

FIGURE 19: Maximum reflected power seen by the window.

Another feature of the window requirements is as follows. The reflection of the power from the cavity due to coupling mismatch ($\beta \neq 1$) comes from a fixed reflection point, the coupling iris. This means that the VSWR phase pattern is spatially fixed in the input waveguide. Knowing where the voltage maximums and the current maximums are located along the waveguide, the window can be placed at the most advantageous position for its survival.

To accommodate the higher power levels, it was decided to investigate the feasibility of a planar waveguide vacuum window.

The proposal of Gamma Microwave was chosen for development.[23] The window that they designed incorporates the following features:

- WR1800 Planar Waveguide window.
- Beryllium Oxide ceramic.
- All metal parts are copper or Stainless, no Kovar.
- The Ceramic is brazed directly to Copper.
- The window has anti multipacting coating.
- The unit is water cooled.
- The unit is compatible with vacuum baking.
- The vacuum side is reduced height WR1800.

Beryllium oxide has a factor of 10 higher thermal conductivity than the more customary window ceramic, alumina, improving the prospects for handling the higher power envisioned. The reduced height waveguide is compatible with the input coupler design. A drawing of the window is shown in Fig. 20.

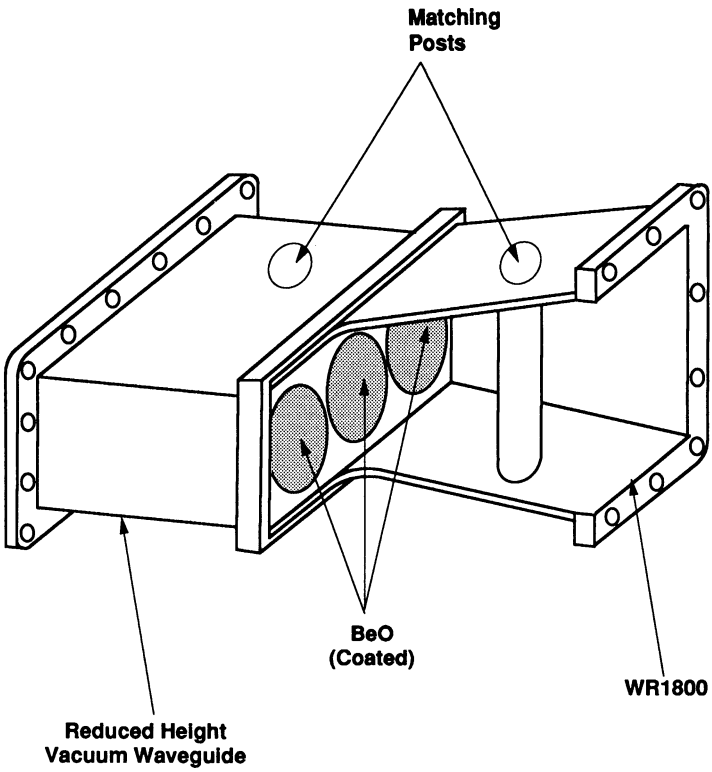

FIGURE 20: Planar waveguide high power window under development.

On receiving the window, low power measurements were made using a Network Analyzer, a WR1800 full height to half height taper and WR1800 to type N adapters. Measurements were made of VSWR, transmission, and phase shift of each window as a function of frequency. The VSWR was less 1:1.05 over ± 5 MHz, there was no measurable transmission loss, and the phase shift was a smooth function of frequency.

As a first medium power test, the window was assembled in the configuration shown in Fig. 21 and tested with 220 watts of power.

The resonant circulating power at the window was 26.8 Kwatts, 13.4 Kwatts in each direction. The maximum temperature rise of the window cooling water was less then 3 degrees C. The vacuum base pressure before the test was 6×10^{-9} torr. During the test the maximum measured pressure was 7×10^{-9} torr. Some temperature rise was observed in the hollow matching posts or tubes on each side of the ceramic. During this test the posts were near a current maximum.

Future high power tests are planned to include two windows and a high power transmitter consisting of a 500 Kwatt Klystron, a high power circulator and a 500 Kwatt high power RF load. These 500 Kwatt tests have not yet been completed. For the 500 Kwatt tests, the matching posts will be cooled with circulating water.

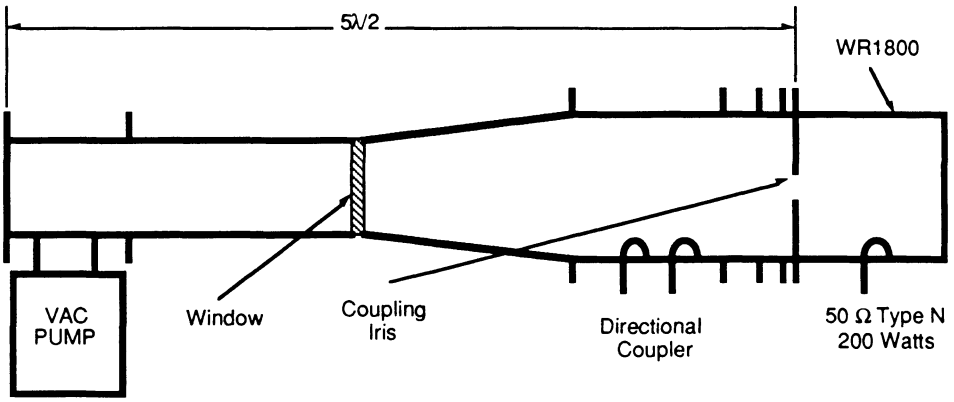

FIGURE 21: Medium power test configuration.

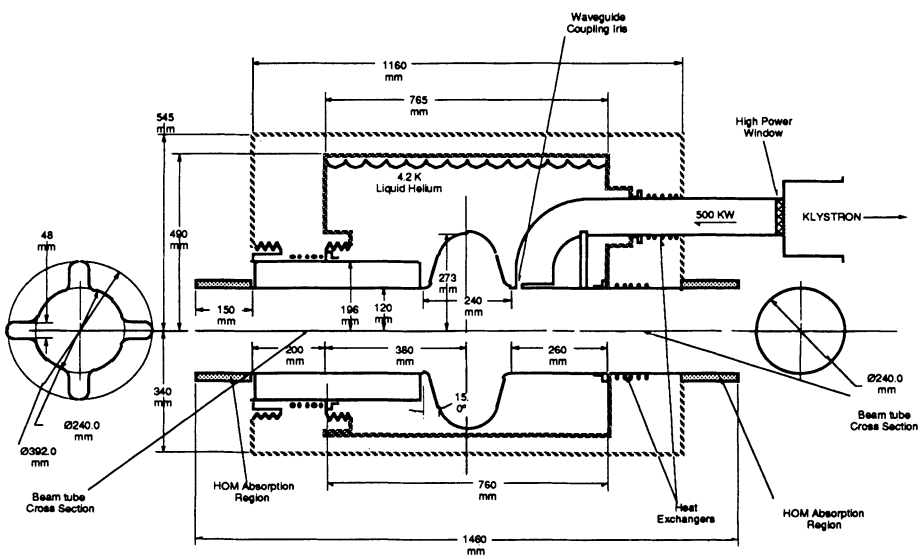

FIGURE 22: Complete concept of a superconducting cavity for a high luminosity storage ring.

9 SUMMARY

With successful operation in TRISTAN, LEP, and HERA, superconducting cavities become attractive for use in high luminosity machines, where lowering machine impedance is of prime importance to storing amps of beam current in many closely spaced bunches. We have developed an advanced storage ring cavity design (Fig. 22) in which all important higher modes propagate out of the cavity via a specially shaped beam pipe. The beam pipes are the higher mode couplers. Outside the cryostat, a ferrite absorber, made as a part of the beam pipe lowers the Q of all higher order modes to below 200, with most below 100. A waveguide input coupler is developed and a high power planar waveguide window is under test.

REFERENCES

1. M. Tigner, (1990). European Particle Accelerator Conf. (1990).
2. D. Rubin et al, (1989). Proc. of the 1989 Particle Accelerator Conf., IEEE Cat. No. 89CH 2669-0, 1837.
3. W. Chou, (1991). SSC, private communication.
4. CESR-B, Conceptual Design Report, CLNS 91-1050.
5. D. Rubin, (1990). AIP Conf. Proc. 214, A.M. Sessler, Ed.
6. K. Akai, (1991). Proc. Fifth Workshop on RF Superconductivity, Hamburg, Germany, 126.
7. S. Noguchi, (1990). 1990 European Particle Accelerator Conf.
8. K. Akai, (1989). Proc. of the 4th Workshop on RF SC, Y. Kojima, Ed., KEK Report No. 89- 21.
9. U. Laustroer et al, (1987). DESY-87 – 03.
10. T. Weiland, (1983). Nucl. Instr. and Methods in Phys. Res. 212, 13.
11. G. Arnolds-Mayer, (1988). Proc. of the 3rd Workshop on RF SC, Ed. K. Shepard, ANL- Phy-88-1, 55.
12. Kageyama, (1990). KEK B-Factory Workshop, Oct. 1990.
13. R. Klatt et al, (1986). Proc. of the 1986 Linac Conf., SLAC Report 303, 276.
14. K. Halbach and R.S. Holsinger, (1976). Particle Accelerators, **7**.
15. M.S. deJong and F.P. Adams, (1990). Proc. of the CEFC '90 Conference, Toronto, Canada, Oct. 1990.
16. M. Zisman et al, (1986). LBL-21270 ESG-15.
17. Conceptual Design Report for the SLAC/LBL B-Factory, SLAC-372. (1991).
18. P. Wilson and J.E. Griffin, (1981). AIP Conf. Proc. No. 87, 450.
19. HP Product Note 8510-3, August 1985.
20. W. Barry, (1986). IEEE Trans. Microwave Theory and Techniques, MTT34(1), 213.
21. W. Bauer et al, (1983). IEEE Trans. Nucl. Sci. 30, 3333.
22. S. Noguchi et al, (1980). KFK #347/80.
23. R. Gerlack, Gamma Microwave, Santa Clara, Ca 95054.

APPENDIX Parameter List for CESR-B

Parameter	HER	HER & LER	LER
E [GeV] (beam energy)	8.0		3.5
$\mathcal{L}$ [10^{33} cm^{-2}s^{-1}] (luminosity)		3.0	
$(\xi/\beta_V^*)(1+r)$ [m^{-1}] (luminosity coefficient)		2.0	
n_b (number of bunches)		230	
r (aspect ratio)		0.015	
N [10^{11}] (e/bunch)	0.60		1.37
Itot [A] (current in one beam)	0.87		1.98
Circumference [m]		764.84	
β_H^* [m] (IP focussing parameter)		1.0	
β_V^* [cm]		1.5	
θ_c [mrad] (crossing angle)		12.0	
σ_L [cm] (bunch length)		1.0	
ϵ_H [10^{-7}m] (emittance)		1.3	
$\alpha[10^{-2}]$ (momentum compaction)	0.84		1.1
η^* [m] (dispersion at IP)		0.0	
Qs (synchrotron tune)		0.085	
Q_H (betatron tune)	12.7		11.7
$\sigma_E/E[10^{-4}]$ (energy spread)	8.4		6.5
U_o [MeV/rev] (SR energy loss)	5.23		0.76
P_{SR} [MW] (SR power per beam)	4.5		1.5
V_c [MV] (cavity voltage)	35		11.9
U_c [MV] (crab voltage)	1.8		0.8
β_{crab} [m]		25	
P_{hom} [kW] (per beam)	67		180
n_c (number of SC cavities per ring)	12		4
P_{rf} [MW] (available rf power)	4.8		2.4
λ_{rf} [cm] (rf wavelength)		60	
τ_ϵ [ms] (energy damping time)	3.9		11.7
$\tau_{x,y}$ [ms] (betatron damping time)	7.8		23.4
Q_L (loaded Q of cavity acc. mode $/10^5$)	2.6		2.7